Atmos. Chem. Phys. Discuss., 14, 20805–20844, 2014
www.atmos-chem-phys-discuss.net/14/20805/2014/
doi:10.5194/acpd-14-20805-2014

Atmospheric Chemistry and Physics Discussions

Daily global fire radiative power fields estimation from one or two MODIS instruments

S. Remy[1] **and J. W. Kaiser**[1,2,3]

[1]European Centre for Medium-range Weather Forecasts, Chemical Aspects Section, Reading, UK
[2]King's College London, London, UK
[3]Max-Planck-Institut für Chemie, Mainz, Germany

Received: 22 April 2014 – Accepted: 14 July 2014 – Published: 12 August 2014

Correspondence to: S. Remy (samuel.remy@ecmwf.int)

Published by Copernicus Publications on behalf of the European Geosciences Union.

Abstract

Fires are important emitters of aerosol and trace gases and as such need to be taken into account in any atmospheric composition modeling enterprise. One method to estimate these emissions is to convert Fire Radiative Power (FRP) analysis to dry matter burnt and emissions of smoke constituents using land cover dependent conversion factors. Inventories like the Global Fire Assimilation System (GFAS) follow this approach by calculating daily global smoke emissions from FRP observed by the MODIS instruments on-board of the Terra and Aqua satellites. Observations with different overpass times systematically sample fires at different stages in the strong diurnal fire cycle. For some time periods, observations are available from only one instrument, which leads to a bias in the observed average FRP.

We develop a method to correct this bias in daily FRP observations from any Low Earth Orbit (LEO) satellite, so that the budget of daily smoke emissions remains independent of the number of satellites from which FRP observations are taken into account. This ensures the possibility of running, e.g., GFAS in case of a default of one of the MODIS instruments. It also enables the extension GFAS to 2000–2002 and the inclusion of FRP observations from upcoming satellite missions. The correction combines linear and non-linear regressions and uses an adaptive regionalization algorithm. It removes the bias in daily average FRP observations from Terra and Aqua nearly entirely. Errors are larger for Terra than for Aqua, are generally relatively small at a global scale, but can be important at a local scale. The correction algorithm is applied to Terra observations from 25 February 2000 to 31 December 2002, when Aqua observations were not available. The database of fire emissions GFASv1.0 is extended correspondingly.

ACPD
14, 20805–20844, 2014

1 Introduction

1.1 Importance of biomass burning emissions in atmospheric composition modeling

Vegetation fires are a frequent occurrence in all vegetated environments. They are ignited naturally (i.e. by lightning) or by anthropogenic activity. They can be the cause of serious public health issues such as the extreme Particulate Matter (PM) concentrations recorded in Singapore at the end of June 2013, caused by fires in neighboring Sumatra island[1]. Depending on the vegetation cover, fires emit various aerosols, reactive gases and greenhouse gases. More specifically, fires are a major source of black carbon in the atmosphere: they are responsible for around 40 % of the emissions of Carbon Monoxide (CO), a precursor gas for Ozone (O_3). They are also an important source of Nitrogen oxides (NO_x). As such, biomass burning emissions play an important role in chemical composition and air quality forecasts.

Fires also affect the radiative balance of the atmosphere by emitting greenhouse gases such as Carbon Dioxide (CO_2) and Methane (CH_4). They also release large quantities of aerosol particles such as Black Carbon (BC) and Organic carbon (OC), which in turn impact the atmosphere through the aerosol-radiation and aerosol-cloud interactions. Diehl et al. (2012) estimate the global OC emissions from biomass burning as 14–57 Tg year^{-1}, while BC ranges from 1.8 to 7 Tg year^{-1}. Bond et al. (2013) cite ranges of 2–11 Tg (BC) and 18–77 Tg (organic carbon) for the global annual estimates of emissions from open biomass burning. Out of 13 identified radiative forcing agents (Bowman et al., 2009), 8 are impacted by fires. Therefore, taking into account the contribution of fires in the global emissions of aerosols, reactive gases and greenhouses gases is a necessary step in any global modeling of atmospheric composition enterprise. Since fires occur mostly in locations where in-situ observations are not available and are characterized by a large temporal and spatial variability, assessing their size

[1] See http://www.gmes-atmosphere.eu/news/singapore_smoke

ACPD
14, 20805–20844, 2014

and intensity requires the use of remote observations. Most fires are characterized by a strong diurnal cycle, e.g. Giglio (2007), Roberts et al. (2009), often with a maximum in the early afternoon. Satellite observations of the currently active fires are the only source that can provide a global estimation of fire activity. Several systems that calculate the biomass burning emissions from satellite observations of burnt area or active fire areas have been developed over the recent years (van der Werf et al., 2006, 2010; Freitas et al., 2005; Reid et al., 2009; Sofiev et al., 2009; Kaiser et al., 2009, 2012).

The European Union funded project "Monitoring Atmospheric Composition and Climate – Interim Implementation" (MACC-II) provides global analysis and forecasts of atmospheric composition, alongside European air quality forecasts (Hollingsworth et al., 2008). In order to provide this forecasting system with accurate estimates of aerosol, reactive gases and greenhouse gas emissions from biomass burning, the Global Fire assimilation System (GFAS, Kaiser et al., 2009) based on satellite-based fire radiative power (FRP) observations has been developed. GFAS grids and averages FRP observations from the MODIS instrument onboard NASA's Terra and Aqua satellites. This gridded data from the two satellites are then merged to produce global daily averaged FRP fields with 0.5 and 0.1° resolutions. An analysis of daily averaged FRP is then built by assimilating this merged daily averaged FRP observation. The assimilation step consists of a simple Kalman filter used with a persistence model; its objective is to fill the observational gaps, caused mainly by cloudy conditions.

Heil et al. (2010) found strong correlations between FRP and the dry matter combustion rate of the Global Fire Emission Database (GFED, van der Werf et al., 2010) v3.1. This allowed the derivation of conversion factors for eight land cover classes that link GFAS FRP to GFED dry matter combustion rate, which allows GFAS to provide a global analysis of dry matter burnt. Emission factors following Andreae and Merlet (2001) are then used to estimate the emissions of 41 species from the dry matter burnt estimate. As GFAS translates a daily averaged FRP into a daily average emission rate of species (Kaiser et al., 2012), it contains no information about the diurnal cycle of

ACPD
14, 20805–20844, 2014

biomass burning emissions. Our aim here is to try to reproduce this daily average FRP and biomass burning emissions using one source of observations instead of two.

The MACC-II project also produced an 8 years reanalysis (Inness et al., 2013) of global atmospheric composition, using biomass burning emissions estimates from GFED and GFAS. The biomass burning emissions database was then extended from 1 January 2003 to the current day. Besides its every-day use in the MACC-II global atmospheric composition forecasts, this database attracts a growing number of users worldwide.

1.2 Satellite observations used in real-time emission calculation

Only low-earth-orbiting (LEO) satellites provide full global observational coverage and the Moderate Resolution Imaging Spectroradiometer (MODIS) instruments on-board NASA's polar orbiting satellites Aqua and Terra are the only instruments for which fire products are currently provided in real-time (Giglio et al., 2003, 2006). The FINN (Wiedinmyer et al., 2011) and FLAMBE emission inventories Reid et al. (2009) use hot spot observations from MODIS. Other real-time inventories, i.e. GFAS, QFED (Darmenov and da Silva, 2013) and IS4FIRES (Sofiev et al., 2009) use the additional quantitative information of the Fire Radiative Power (FRP) products from the MODIS satellites. Both observations are only available for clear-sky conditions, and show a decreasing accuracy as the viewing angle increases (Freeborn et al., 2011). The Terra overpass time is around 10:30 LST in its descending mode and 22:30 LST in its ascending mode. The Aqua overpass times are around 13:30 LST (resp. 01:30 LST) in ascending (resp. descending) mode.

The diurnal fire cycle is reflected in a significant bias in the FRP observations from the two MODIS instruments (Giglio, 2007; Roberts et al., 2009). This bias has a strong geographic dependency because the diurnal cycle of fire intensity depends on the land cover type: for example, peat fire's intensity hardly vary between day and night while savannah fires nearly extinguish at night. Accurate emission inventories need to combine as much information as possible. For example, GFAS currently merges observations

ACPD
14, 20805–20844, 2014

from Aqua and Terra, weighted by the observed area product, which depends on the cloud cover. That means that the relative signal from both satellites in the final GFAS FRP analysis is varying from day to day. To sum up, the difference between Terra and Aqua FRP can be caused by the diurnal cycle of fires and by a change in cloudiness between their overpass times.

While running GFAS with FRP observations from only Aqua or Terra is technically feasible with the current configuration, the above shows that if we want to ensure that the daily averaged FRP and biomass burning emissions are coherent with the classical configuration (i.e. assimilating data from both satellites), a correction step is required. This also applies to other emission inventories that use MODIS observations with a temporal resolution of one day or more. Availability of only one MODIS instrument occurs in three situations: before the launch and start of product generation from Aqua (February 2000–December 2002), during short breaks in the real-time availability of one or the other MODIS instrument, and, in the future, after the lifetime of whichever instruments fails first.

1.3 Objectives of this work

The objective of this work is to develop a method that can adequately correct the FRP products from LEO satellites such that daily averaged FRP, and thus biomass burning emission, estimates remain unbiased between time periods with all satellites available. The method will be derived for MODIS observations from the Terra and Aqua satellites, but it shall also be applicable for VIIRS and Sentinel-3 observations. It will be used to extend the GFAS emission inventory back to 2000. It will also provide resilience of GFAS against failure of one of the MODIS instruments, and prepare for the ingestion of FRP products of NPP VIIRS and Sentinel-3 SLSTR in as soon as they become available in real time.

Ellicott et al. (2009) succeeded in using observations from Terra only to estimate monthly averaged FRE, with only a small bias from using observations from Aqua and Terra. The system used in their work was rather different from GFAS, as it estimated

ACPD
14, 20805–20844, 2014

a diurnal cycle based on geostationary satellites and didn't include a data assimilation step to fill observational gaps. Our aim is however to reach the same results with daily averaged FRP and biomass burning emissions.

2 Methods

2.1 Overall approach

Since fires vary so much both spatially and temporally and the relative contribution of Aqua and Terra FRP observations to the final product vary from day to day, it is not realistic to aim to reproduce the local and temporal variability of fires as sampled by two sources of observations when running with only one source. Also, cloudiness changes and the diurnal cycle of fires introduce differences between Aqua and Terra. We will focus here on trying to compensate the effect of the diurnal cycle on observed FRP. A statistical regression fit from a learning dataset will be used, the quality of its output will be assessed using an independent verifying dataset.

2.2 Choice of variables

GFAS assimilates merged FRP observations in a 24 h window to produce a best estimate of the daily average FRP, from which emissions of various gases and aerosols are derived. We will work on these daily FRP observations instead of FRP analysis from GFAS or directly on the emissions. As global observations from Aqua or Terra are collected within a 12 h span, it makes sense to use a longer period for our explanatory variable: a 24 h period is the best choice as it allows us to directly apply the correction to the merged observations that are assimilated in GFAS. For the same reason, it was preferred to scale daily observations of Terra (resp. Aqua) toward merged FRP from both satellites instead of towards observations from the other satellite.

ACPD
14, 20805–20844, 2014

2.3 Learning and verification datasets

The learning dataset is composed of daily averages of FRP from Aqua and Terra, averaged over a 0.5° grid by the GFAS algorithm. It extends from 1 January 2003 to 31 December 2011. To prevent taking into account situations where Aqua and Terra observations are very different, because of a change in cloudiness for example, fires for which the ratio of Terra- or Aqua-GFAS over Full-GFAS was above the ninth decile of the whole dataset for the considered day were not included in the dataset. The effect of this exclusion was shown to be very positive as measured by the correlation coefficient between the datasets.

The diurnal cycle, and thus the physics underlying the statistical link between FRP observations from Aqua and Terra, depends on the land cover; therefore an application of a regression algorithm to global FRP needs to take this dependency into account. Also, fire typology varies a lot from region to region. Tropical regions dominated by large forests and savannah exhibit large seasonal fire activity that is long-lasting and relatively regular. These regions contribute a lot to global FRP. Boreal regions with forests mostly composed of coniferous trees are on the other hand subject to fire events that are much more irregular in size and intensity. A few large events such as the Rim fire of August 2013 in California, or the Quebec fires of June and July 2013[2] that sent a plume crossing the Atlantic and affecting Europe can have a significant impact on global FRP (see also Dahlkötter et al., 2014). To be able to take into account this geographical variability in fire activity patterns and the impact of different land covers, regression needs to be applied to regional subsets of the learning dataset instead of a global one.

The verification dataset extends from 1 January 2012 to 31 December of the same year.

[2] See http://www.gmes-atmosphere.eu/news/canada_smoke and http://www.wunderground.com/blog/JeffMasters/canadas-2nd-largest-fire-on-record-spreading-smoke-to-europe

ACPD
14, 20805–20844, 2014

2.4 Two different regionalization strategies

The sample size for every considered local datasets needs to be large enough for a regression algorithm to be applied safely. A minimal sample size of 400 positive gridded observations of FRP for both Aqua and Terra was chosen. Larger values for this threshold were tested, without much impact on the quality of the regression.

2.4.1 Fixed regions

The regression was applied to $2^\circ \times 2^\circ$ regions across the globe that contained more than 400 fires (as observed by both Aqua and Terra) in the learning dataset. Tests with smaller regions showed that the statistical link between the datasets didn't vary much from one region to another, while many more regions didn't contain enough fires to be considered for regression.

2.4.2 Adaptive regions

In order not to exclude too many regions, an adaptive regionalization algorithm was also tested. If the sample doesn't meet the size criterion for a given $2^\circ \times 2^\circ$ tile, then all fires in a $4^\circ \times 4^\circ$ regions centered on the original tile are considered. If there are still not enough fires in the $4^\circ \times 4^\circ$ region, then fires are considered in a $6^\circ \times 6^\circ$ region, and so on, up to a maximum area of $12^\circ \times 12^\circ$. Figure 1 shows the comparative areas that meet the sample size criterion for the two regionalization methods. It is clear from this figure that the "adaptive regionalization" algorithm allows us to apply regression to nearly the whole globe instead of a much smaller domain when using only $2^\circ \times 2^\circ$ domains. The regions where fires are very common, and especially the tropical forests and savannahs, are prominent in Fig. 1 when using fixed regions. A few regions that meet the sample size criterion lie in desert areas, such as at the border between Tunisia and Algeria or in South-West Iran. These could be due to fires coming from gas extraction

ACPD
14, 20805–20844, 2014

facilities that were not masked in GFAS. The comparative advantage of this regionalization strategy will be assessed in next section.

2.5 Regression approaches

2.5.1 Linear regression

The linear regression algorithm was applied to the two set of regions described above and to the learning dataset that extends from 2003 to 2011. The algorithm consists of computing for every region, the linear regression coefficient a, and a coefficient b, such that:

$$\|Y - (a \cdot X + b)\| \quad (1)$$

is minimal. X is the sample of 0.5° daily FRP from Aqua or Terra contained in the considered region (i.e. the explanatory variable), and Y is the sample of 0.5° FRP merged from both Aqua and Terra (i.e. the dependent variable). The correlation of the two variables will be evaluated on the learning dataset using the square of the correlation coefficient r^2. The skill of the regression will be assessed on the verification dataset by comparing the output of GFAS when assimilating corrected and uncorrected daily FRP from either Aqua or Terra. This comparison will be carried out by means of checking the bias and the Root Mean Square Error (RMSE) against GFAS used in the classical configuration, i.e. assimilating merged observations from both Terra and Aqua.

2.5.2 Nonlinear regression

Three different kinds of nonlinear regression formulae were tried, the polynomial $\sum_i a_i x^i$, the hyperbolic $\sum_i \frac{a_i}{x^i}$ and the exponential ae^{bx} or ax^b where a, a_i and b are parameters that are adjusted to find the best fit. Combinations of the three families were also tried, and it was shown that the approach that minimized the distance between

ACPD
14, 20805–20844, 2014

the corrected daily FRP and the merged FRP was to combine a polynomial and the hyperbolic function:

$$F(X) = aX^4 + bX^3 + cX^2 + dX + \frac{e}{X} \quad (2)$$

where the five parameters a, b, c, d and e are determined for each region by minimizing the least square distance between Y and $F(X)$ using the Levenberg–Marquardt algorithm (Marquardt, 1963). Figure 5 shows the relative improvement brought by the non-linear regression relatively to the linear regression as applied to the learning dataset, in terms of distance to merged daily FRP. In many areas, the improvement is in the order of 10 to 20 %. Regions where the improvement is larger do not always coincide with regions where the correlation coefficients are small, as shown on Fig. 4. Also, the non-linear regression appears to improve the regression slightly more for Terra than for Aqua by far.

2.5.3 Combined regression

It is also possible to combine the linear and non-linear approaches when correcting the verification dataset. As the non-linear algorithm is less stable, for larger values of FRP the linear regression is preferred while for smaller values non-linear regression is applied. The threshold between the two needs to be adaptive as outlying values are very time and space-dependent. It was chosen to depend percentile of the whole daily FRP dataset for the considered dataset. A sensitivity study was carried out as to what percentile fives the best results depending on which satellite observations are being corrected; its results are shown in the results section.

2.5.4 Distance metrics

In order to compare the results from linear, non-linear regressions and combined approaches, a common distance metric needs to be defined to be able to measure the

ACPD
14, 20805–20844, 2014

efficiency of each algorithm. The classical regression coefficient is only applicable to linear regression algorithm. The approach chosen here is to compare, for each regional dataset, the norms of the vector composed of the difference between the regression and the dependent variable, i.e.

$$\|\boldsymbol{Y} - F(\boldsymbol{X})\| = \sqrt{\left(\sum_i (\boldsymbol{Y}_i - F(\boldsymbol{X}_i))^2\right)} \quad (3)$$

where $\boldsymbol{Y}$ is the dependent variable vector, i.e. Full GFAS here, composed of a sample of $\boldsymbol{Y}_i$ scalars, $\boldsymbol{X}$ is the explanatory variable vector, i.e. Aqua or Terra GFAS, and F is the linear or non-linear regression algorithm applied to every component $\boldsymbol{X}_i$ of this vector. This distance is not normalized by the size of the dependent variable vector; that means that its value depends also on the size of this vector. As we used this distance only to compare the various algorithms that were tried, this is not an issue here.

3 Results with the verification dataset

In this section daily FRP from the verification dataset are corrected by the different regressions shown above and then assimilated in Terra- and Aqua-GFAS. Table 1 shows the global daily FRP averaged over the verification dataset, as computed by GFAS using observations from both Terra and Aqua, from Aqua only and from Terra only. The important bias of GFAS when running it with observations from only one satellite without any correction is very apparent in this table and gives an indication on the importance of the correction that needs to be made.

3.1 Linear regression

The linear regression was applied to regional datasets corresponding to fixed $2 \times 2^{\circ}$ regions with more than 400 fires, and to regional datasets provided by the adaptive regionalization algorithm.

ACPD
14, 20805–20844, 2014

3.1.1 Results with the fixed regionalization

Figure 2 shows the square of the correlation coefficient for the daily Aqua or Terra FRP against merged FRP. The square of the correlation coefficient is much higher for Aqua (values lie between 0.85 and 1) than for Terra (values generally lie between 0.5 and 0.8). This is not really surprising, considering that the overpass time of Aqua is generally closer to the fire activity peak. As such, Aqua FRP observations are usually larger than Terra's and correlation of Aqua daily FRP with the merged FRP is also larger.

For the same reason, the regression coefficient (not shown) is generally below one for Terra and above one for Aqua. However, the values are very different from one region to the other, in both cases. The differences between the main groups of regions can be explained in terms of land cover, using the MODIS-based MCD12 land cover map version 5.1, shown in Fig. 3 for the year 2005 (Olofsson et al., 2012; Stehman et al., 2012). Regions with relatively higher regression coefficients, such as Northern Australia and South America are predominantly savannah regions, while regions with woody savannah display lower regression coefficients (Africa, south of the Equator). Grasslands, like the ones that can be found in Africa, north of the Equator, are in an intermediate position. An explanation for this different behaviour could lie with the different diurnal cycles associated with each of these land cover type, which could be a cause for the difference between fire intensity as observed by Terra in the morning and by Aqua at midday (Giglio, 2007; Roberts et al., 2009, for example).

For a simpler reading in the following subsections, GFAS FRP obtained assimilating only Aqua (resp. Terra) FRP data from the verification dataset will be called "Aqua (resp. Terra) GFAS", while the reference GFAS FRP, obtained assimilating FRP data from both satellites will be called "Full GFAS".

Table 1 shows the global averaged RMSE and bias of the linear regression correction for Aqua GFAS and Terra GFAS as compared to Full GFAS. The global average FRP is also indicated and can be compared to the global average FRP from GFAS when

ACPD
14, 20805–20844, 2014

running with uncorrected daily FRP observations from Terra or Aqua. When the correction was not available, because the sample was too small for example, uncorrected values of daily FRP were used.

Comparing the results from Table 1 shows that for both Aqua GFAS and Terra GFAS, using daily FRP corrected by linear regression is rather efficient in bringing the average FRP closer to our reference. Using the corrected daily FRP reduced the bias by a factor of three for both Aqua- and Terra-GFAS. The RMSE is quite high for both cases, with values that are 20 to 25 % of the average FRP for Aqua GFAS and Terra GFAS respectively. This relatively high level of error can be partially explained by the bias, which represents more than half of the RMSE in both cases.

This first result is encouraging though not entirely satisfying, because of the remaining bias and the relatively high level of RMSE.

3.1.2 Results with the adaptive regionalization algorithm and comparison with fixed regions

Figure 4 shows the square of the correlation coefficient of Aqua or Terra daily FRP with merged FRP, using the adaptive regionalization algorithm. In the regions where fires are common, the same features as with the fixed regions are displayed. In other regions, the impact of the land cover type is clearly shown: savannah and grassland regions in particular (United States, Australia outside the Northern rim, Africa around the Northern Tropics) have very similar values. Boreal forests display regression coefficient (not shown) values close to one, for both Aqua and Terra. This can be explained by the fact that fires in these regions occur not as frequently as in the tropical forests, but usually with a higher intensity. Intense fires tend to also burn during the nights and to limit the amplitude of the diurnal cycle. The correlation coefficients display larger values for Aqua daily FRP as compared to Terra daily FRP, for reasons already explained. The values are very close to one in most of the regions where fires were considered in a larger area than the original $2^{\circ} \times 2^{\circ}$ region. This means that enlarging the sample

ACPD
14, 20805–20844, 2014

was not detrimental to how much the explanatory and the dependent variables are correlated in these regions.

Comparing the results with fixed and adaptive regions in Table 1 shows that the RMSE of the scaled Aqua-GFAS is reduced by nearly a factor of two when using the adaptive regionalization algorithm, and by more than ten percent for Terra-GFAS. The bias is nearly entirely eliminated for Aqua-GFAS and reduced by a fourth for Terra-GFAS. These results show that including regions where fires are not as common as in the fixed regions help a lot in improving the quality of the regression. The global average of FRP show that the regression nearly entirely eliminates the bias that was caused by using observations from only one satellite.

3.2 Nonlinear regression and combined approach

Nonlinear regression was applied only to datasets provided by the adaptive regionalization algorithm, as it was shown that this algorithm improves significantly the quality of the regression. Using only the non-linear regression to correct observations brought a marked degradation when using these observations in GFAS. This degradation is caused by the fact that non-linear regression gave extreme results for a few fires with large FRP: this algorithm is much less stable as compared to linear regression.

3.2.1 Reasons for using the combined approach

As we are dealing with datasets that are very varied, with weaker or stronger statistical links between them, a non-linear regression will be more efficient in capturing the statistical link between Aqua and Terra daily FRP on one hand and merged daily FRP on the other hand. This is clearly shown by Fig. 5. The relative improvement brought by the non-linear approach as compared to the linear one is mostly evident in regions where fires are less common and as a consequence where the adaptive regionalization algorithm provides larger domains, as shown on Fig. 1. Also, the non-linear approach

ACPD
14, 20805–20844, 2014

seems to have a larger positive impact for Terra as compared to Aqua as shown by Fig. 5.

However, the non-linear formulae cannot be applied to the verification dataset without removing the outlying data. The non-linear algorithm works overall better, but for very large daily FRP from Terra or GFAS, or if the difference between Aqua and Terra is too large because of difference cloud cover conditions, non-linear regression can bring very large errors. In particular, applying the non-linear approach to daily FRP that lies outside of the learning dataset will give very poor results; while the linear approach is safer in this case. This is clearly shown by Fig. 6: if the non-linear approach is applied to large values, then the result will be extremely large (for the region considered in the right part of the figure), or even negative for the region considered on the left.

A way to exploit both the robustness of the linear algorithm and the added skill of the non-linear approach was found by designing and applying the combined algorithm that has been explained in the methods section. Several values for the daily threshold between the use of linear and non-linear approaches were tested on the verifying dataset. The results of this sensitivity study are summed up in Table 2 for Aqua and Table 3 for Terra. The 100th percentile corresponds to the linear regression being applied only. These tables show a marked difference between Terra and Aqua. For Aqua, the RMSE is decreasing very fast with increasing percentiles, but quickly reaches a floor. Bias however is decreasing more regularly, reaches a minimum and then increases slightly again. Overall, the non-linear approach is not improving the scores much as compared to the linear regression: the RMSE is the same and the bias is only slightly decreased. For Terra, both RMSE and bias are decreasing and then increasing with the threshold percentiles. RMSE is much larger than for Aqua, and the non-linear approach is more efficient in reducing the bias.

3.2.2 Comparison of the combined algorithm to linear regression

Figure 7 shows daily globally averaged FRP from Aqua-, Terra- and Full GFAS using daily FRP not corrected or corrected by the linear regression and the combined

ACPD
14, 20805–20844, 2014

algorithm applied to the verifying datasets. The high temporal variability of global FRP is very apparent on this figure, as well as how both the linear and combined algorithms are successful overall in scaling both Aqua-GFAS towards Full-GFAS, except for a few large fire events such as in March and April 2012 and also at the end of October 2012. The differences between the linear and combined approaches are very small. For Terra-GFAS, the regression is overall less successful, in particular up to 1 May 2012. The daily FRP as provided by GFAS using observations corrected by the combined algorithm is generally slightly larger as compared to the values obtained with the linear regression. As shown also by Table 3, applying linear-regression is having a greater impact on Terra than on Aqua.

The apparent difference between the small improvement brought by the combined regression when applied to the verifying dataset and the larger reduction of the distance brought by the same method when applied to the learning dataset (see Fig. 5) can be explained by the fact that the regions where the combined algorithm reduces this distance the most are the regions where fires are less common. The tropical forests and savannahs, which contribute generally the most to the global FRP, do not show a large improvement of the combined method as compared to linear regression on Fig. 5. This shows that non-linear regression has most impact on fires in regions that generally contribute much to global FRP, so that this improvement is not very visible when considering daily global FRP, even though it is locally important.

Figure 8 shows daily FRP from Aqua-, Terra- and Full GFAS, averaged over Africa, Indonesia, South and North America. GFAS output using observations not corrected and corrected with the combined algorithm are shown. This figure clearly shows the varying ratio Aqua over Terra from region to region: it is large in Africa, and rather small in North America.

A spurious oscillation of daily FRP as estimated by Aqua observations, with a two day frequency, is very prominent in Africa. This is caused by the fact that the detection threshold of the MODIS sensor varies across the swath. It increases with viewing angle, towards the swath edges (e.g. Freeborn et al., 2011); this leads to lower FRP estimates

ACPD
14, 20805–20844, 2014

in GFAS for grid cells that are observed nearer the MODIS swath edges as smaller fires are not taken into account. As for both Aqua and Terra there are fewer overpasses around the equator, this results in an underestimation of FRP every two days. This shows more clearly for Aqua, because it captures better the maximum intensity of fires thanks to its overpass time. This underestimation in the FRP analysis over Africa is compensated by the fact that the conversion factors to convert FRP into dry matter burnt were computed using monthly average FRP from GFAS and monthly average dry matter combustion rates of GFED (Andela et al., 2013). This issue will be addressed in the next version of GFAS, which will include a correction of FRP observations to account for the detection threshold of MODIS as a function of the viewing angle. The algorithm of this correction is exposed in detail in Kaiser et al. (2013).

Figure 8 also shows that the correction algorithm is very efficient in bringing both Terra- and Aqua-GFAS towards full-GFAS, for the four considered regions. For South America, the relative improvement brought by the correction appears more important for Aqua-GFAS than for Terra-GFAS.

To focus to a local scale, Fig. 9 shows the impact of both methods on a particular fire event, in West Africa, on 3 April 2012. The daily FRP analysis from GFAS using the original Terra dataset shows values that are largely inferior to merged FRP whereas they superior for the original Aqua dataset. The observed area (not shown) are comparable for both satellites on that day, which means that different cloudiness between the Terra and Aqua overpass times is not the cause of this very important difference. This fire event contributed significantly to global FRP on that day, and as Fig. 7 shows, the regression was not very successful on that particular day on a global scale. The causes of this relative lack of success are clear when considering the difference between Terra-GFAS and Aqua-GFAS, even when using daily FRP from Terra that have been corrected. For this particular example, the combined approach scales FRP from Terra-GFAS closer to Full-GFAS as compared to linear regression. The different behaviour of both regression methods from one region to another is clear when

ACPD
14, 20805–20844, 2014

considering that the maximum FRP doesn't occur in the same grid cell once either regression method is applied.

This figure shows that at a local scale, errors are reduced by the regression but can still remain large. It also shows that the differences from the linear and combined regressions are larger when considered at a local scale.

Figure 10 shows how both regression algorithms perform at a local scale on 23 October 2012, for fires in Australia that were an important contribution to the peak of global FRP that was observed that day, as shown on Fig. 7. The difference between the FRP analysis from Full-GFAS, Terra-GFAS and Aqua-GFAS using non-corrected data are visible but much less important than in the other case. As a result, the regression is much more efficient in producing daily FRP that bring Terra-GFAS and Aqua-GFAS FRP analysis closer to Full-GFAS. The non-linear approach doesn't have any visible impact in that case.

4 Extension of the GFAS emissions database

The combined linear and non-linear approach was applied to Terra-GFAS for the period extending from 24 February 2000 to 31 December 2002. Static correction (volcanoes, gas flares) and quality control were carried out as described in Kaiser et al. (2012): all observations with a daily FRP value above 20 W (average for a 0.5° grid cell) per square meter was not taken into account.

Figure 11 shows Terra-GFAS using uncorrected daily FRP from Terra, values corrected with linear regression and non-linear regression. The correction brings larger GFAS FRP analysis: the mean daily global FRP for the 24 February 2000 to 31 December 2002 period is 1.79×10^{-4} mW m^{-2} when using uncorrected Terra daily FRP, 2.31×10^{-4} mW m^{-2} when using corrected Terra daily FRP. These averages are comparable to the values for the year 2012 when using merged daily FRP: 1.486×10^{-4} and 2.238×10^{-4} mW m^{-2}, respectively.

ACPD
14, 20805–20844, 2014

Figure 12 shows monthly global FRP from Aqua, Terra and GFASv1.0, including the extension of GFAS for the period extending from 24 February 2000 to 31 December 2002. While the unavailability of any independent verifying satellite observations makes it impossible to quantitatively assess the accuracy of the corrected FRP, the values for the years 2000 to 2002 show a good agreement with the values afterwards.

The observation products (MOD14) from Terra contain no fire detections for a few periods, especially from 6 to 17 August 2000, from 16 June to 2 July 2001 and from 21 to 29 March 2002. This kind of data fault cannot be detected by the implemented quality control. Therefore, we assume persistence of the fire distribution for these specific dates.

FRP and biomass burning emissions for the period of 1 March 2000 to 31 December 2002 have been added to the GFASv1.0 database, which now encompasses the years 2000–2014. The main differences between GFASv1.0 data before and after 1 January 2003 concerns quality control. Before that, as already mentioned, quality control is applied directly on Terra pixels, whereas after that date quality control consists of a threshold applied to each grid cell of the FRP analysis produced by the assimilation algorithm, as explained in Kaiser et al. (2012).

5 Summary

Several configurations for the correction of Aqua and Terra daily FRP were tried. The adaptive regionalization improves the result of GFAS as compared to the fixed regionalization for both satellites, by a wide margin for Aqua and a smaller one for Terra. The combination of non-linear and linear approaches doesn't bring much improvement for Aqua as compared to linear regression, except for a small reduction in bias. For Terra on the other hand, the RMSE and especially the bias of GFAS are reduced in a significant way when assimilating daily FRP corrected with this combined approach as compared to the linear regression.

ACPD
14, 20805–20844, 2014

Overall, the correction gives better results for Aqua than for Terra. While the correction gives satisfactory results overall at a global scale, errors can be large when considered at a local scale.

6 Conclusions

This paper showed that a combination of linear and non-linear regression manages to remove effectively the bias of the output of GFAS when using observations from only Aqua or Terra. The regression is overall more efficient for Aqua than for Terra, and was designed to address the difference between Aqua and Terra caused by the diurnal cycle of fires. This will ensure the coherence of the output of GFAS at a global scale, should one of these satellites fail. As such, this work consolidated the whole MACC-II system. The GFAS FRP and biomass burning emissions database was successfully extended to the period from 24 February 2000 to 1 January 2003.

As the fire typology varies a lot from one region to the other, an adaptive regionalization algorithm was successfully implemented to design samples that were statistically significant. This allowed us to run the regression in nearly every region of the globe where fires occurred in the past 9 years. For regions where fires were too scarce for the regression algorithms to be run safely, which represent a very small fraction of all fires, the correction exposed here cannot be applied. The approach that was applied here to MODIS observations on Aqua and Terra is also applicable to FRP observations from other sources, i.e VIIRS and SLSTR.

This work also documented the differences between Aqua and Terra FRP observations. These differences are important at a global scale, and even more so at a local scale, as shown by the 3 April 2012 situation in West Africa. Assimilating observations from more instruments, such as geostationary data, will bring more stability to GFAS.

Acknowledgements. We thank NASA for providing the MODIS data. This research was supported by the EU Seventh Research Framework Programme (MACC-II project, contract number 283576).

ACPD
14, 20805–20844, 2014

References

Andela, N., Kaiser, J. W., Heil, A., Van Leeuwen, T. T., van der Werf, G. R., Wooster, M. J., Remy, S., and Schultz, M. G.: Assessment of the Global Fire Assimilation System (GFASv1), available at: https://gmes-atmosphere.eu/documents/maccii/deliverables/fir (last access: 28 July 2014), 2013. 20822

Andreae, M. O. and Merlet, P.: Emission of trace gases and aerosols from biomass burning, Global Biogeochem. Cy., 15, 955–966, 2001. 20808

Benedetti, A., Morcrette, J.-J., Boucher, O., Dethof, A., Engelen, R. J., Fisher, M., Flentje, H., Huneeus, N., Jones, L., Kaiser, J. W., Kinne, S., Mangold, A., Razinger, M., Simmons, A. J., and Suttie, M., Aerosol analysis and forecast in the European Centre for Medium-Range Weather Forecasts Integrated Forecast System: 2. Data assimilation, J. Geophys. Res., 114, D13205, doi:10.1029/2008JD011115, 2009.

Bowman, D. M. J. S., Balch, J. K., Artaxo, P., Bond, W. J., Carlson, J. M., Cochrane, M. A., D'Antonio, C. M., DeFries, R. S., Doyle, J. C., Harrison, S. P., Johnston, F. H., Keeley, J. E., Krawchuk, M. A., Kull, C. A., Marston, J. B., Moritz, M. A., Prentice, I. C., Roos, C. I., Scott, A. C., Swetnam, T. W., van der Werf, G. R., and Pyne, S. J.: Fire in the Earth system, Science, 324, 481–484, 2009. 20807

Bond, T. C., Doherty, S. J., Fahey, D. W., Forster, P. M., Berntsen, T. K., Boucher, O., DeAngelo, B. J., Flanner, M. G., Ghan, S. J., Kärcher, B., Koch, D. and Kinne, S., Kondo, Y., Lohmann, U., Quinn, P. K., Sarofim, M. C., Schultz, M., Schulz, M., Venkataraman, C., Zhang, H., Zhang, S., Bellouin, N., Guttikunda, S., Hopke, P. K., Jacobson, M. Z., Kaiser, J. W., Klimont, Z., Schwarz, J. P., Shindell, D., Storelvmo, T., Warren, S. G., and Zender, C. S.: Bounding the role of black carbon in the climate system: a scientific assessment, J. Geophys. Res., 118, 1–173, 2013. 20807

Dahlkötter, F., Gysel, M., Sauer, D., Minikin, A., Baumann, R., Seifert, P., Ansmann, A., Fromm, M., Voigt, C., and Weinzierl, B.: The Pagami Creek smoke plume after long-range transport to the upper troposphere over Europe – aerosol properties and black carbon mixing state, Atmos. Chem. Phys., 14, 6111–6137, doi:10.5194/acp-14-6111-2014, 2014. 20812

Damenov, A. and da Silva, A.: The Quick Fire Emissions Dataset (QFED) – Documentation of versions 2.1, 2.2 and 2.4, NASA Technical Report Series on Global Modeling and Data Assimilations, 32, 2013. 20809

ACPD
14, 20805–20844, 2014

Diehl, T., Heil, A., Chin, M., Pan, X., Streets, D., Schultz, M., and Kinne, S.: Anthropogenic, biomass burning, and volcanic emissions of black carbon, organic carbon, and SO_2 from 1980 to 2010 for hindcast model experiments, Atmos. Chem. Phys. Discuss., 12, 24895–24954, doi:10.5194/acpd-12-24895-2012, 2012. 20807

Ellicott, E., Vermote, E., Giglio, L., and Roberts, G.: Estimating biomass consumed from fire using MODIS FRE, Geophys. Res. Lett., 36, L13401, doi:10.1029/2009GL038581, 2009. 20810

Freeborn, P. H. and Wooster, M. J., Addressing the spatiotemporal sampling design of MODIS to provide estimates of the fire radiative energy emitted from Africa, Remote Sens. Environ., 115, 2, 475–489, 2011. 20809, 20821

Freitas, S. R., Longo, K. M., Silva Dias, M. A. F., Silva Dias, P. L., Chatfield, R., Prins, E., Artaxo, P., Grell, G. A., and Recuero, F. S.: Monitoring the transport of biomass burning emissions in South America, Environ. Fluid Mech., 5, 135–167, 2005. 20808

Giglio, L., Descloitres, J., Justice, C. O., and Kaufman, Y.: An enhanced contextual fire detection algorithm for MODIS, Remote Sens. Environ., 87, 273–282, 2003. 20809

Giglio, L., Csiszar, I., and Justice, C. O.: Global distribution and seasonality of active fires as observed with the Terra and Aqua MODIS sensors. J. Geophys. Res.-Biogeo., 111, G02016, doi:10.1029/2005JG000142, 2006. 20809

Giglio, L.: Characterization of the tropical diurnal fire cycle using VIRS and MODIS observations, Remote Sens. Environ., 108, 407–421, 2007. 20808, 20809, 20817

Heil, A., Kaiser, J. W., van der Werf, G. R., Wooster, M. J., Schultz, M. G., and Dernier van der Gon, H.: Assessment of the Real-Time Fire Emissions (GFASv0) by MACC, Tech. Memo. 628, ECMWF, Reading, UK, 2010. 20808

Hollingsworth, A., Engelen, R. J., Textor, C., Benedetti, A., Boucher, O., Chevallier, F., Dethof, A., Elbern, H., Eskes, H., Flemming, J., Granier, C., Kaiser, J. W., Morcrette, J.-J., Rayner, P., Peuch, V.-H., Rouil, L., Schultz, M. G., and Simmons, A. J.: Toward a monitoring and forecasting system for atmospheric composition: the GEMS project, B. Am. Meteorol. Soc., 89, 1147–1164, 2008. 20808

Inness, A., Baier, F., Benedetti, A., Bouarar, I., Chabrillat, S., Clark, H., Clerbaux, C., Coheur, P., Engelen, R. J., Errera, Q., Flemming, J., George, M., Granier, C., Hadji-Lazaro, J., Huijnen, V., Hurtmans, D., Jones, L., Kaiser, J. W., Kapsomenakis, J., Lefever, K., Leitão, J., Razinger, M., Richter, A., Schultz, M. G., Simmons, A. J., Suttie, M., Stein, O., Thépaut, J.-N., Thouret, V., Vrekoussis, M., Zerefos, C., and the MACC team: The MACC reanalysis: an 8 yr

ACPD
14, 20805–20844, 2014

data set of atmospheric composition, Atmos. Chem. Phys., 13, 4073–4109, doi:10.5194/acp-13-4073-2013, 2013. 20809
Kaiser, J. W., Suttie, M., Flemming, J., Morcrette, J.-J., Boucher, O., and Schultz, M. G.: Global real-time fire emission estimates based on space-borne fire radiative power observations, AIP Conf. Proc., 1100, 645–648, 2009. 20808
Kaiser, J. W., Heil, A.,Andreae, M. O., Benedetti, A.,Chubarova, N.,Jones, L., Morcrette, J.-J.,Razinger, M., Schultz, M. G.,Suttie, M., and van der Werf, G. W.: Biomass burning emissions estimated with a global fire assimilation system based on observed fire radiative power, Biogeosciences, 9, 527–554, 2012, http://www.biogeosciences.net/9/527/2012/. 20808, 20823, 20824
Kaier, J. W., Andela, N., Atherton, J., de Jong, M., Heil, A., Paugam, R., Remy, S., Schultz, M. G., van der Werf, G. R., van Leeuwen, T. T., and Wooster, M. J.: Recommended Fire Emission Service Enhancements, available at: https://gmes-atmosphere.eu/documents/maccii/deliverables/fir (last access: 25 July 2014), 2013. 20822
Marquadt, D.: An algorithm for least-squares estimation of nonlinear parameters, J. Soc. Ind. Appl. Math., 11, 432–441, 1963. 20815
Olofsson, P., Stehman, S. V., Woodcock, C. E., Friedl, M. A. Sulla-Menashe, D., Sibley, A. M., Newell, J. D., and Herold, M.: A global land cover validation data set, I: Fundamental Design principles, Int. J. Remote Sens., 33, 5768–5788, doi:10.1080/01431161.2012.674230, 2012. 20817
Reid, J. S., Hyer, E. J., Prins, E. M., Westphal, D. L., Zhang, J., Wang, J., Christopher, S. A., Curtis, C. A., Schmidt, C. C., Eleuterio, D. P., Richardson, K. A., and Hoffman, J. P.: Global monitoring and forecasting of biomass-burning smoke: description of and lessons from the Fire Locating and Modeling of Burning Emissions (FLAMBE) program, IEEE J. Sel. Top. Appl., 2, 144–162, 2009. 20808, 20809
Roberts, G., Wooster, M. J., and Lagoudakis, E.: Annual and diurnal african biomass burning temporal dynamics, Biogeosciences, 6, 849–866, 2009, http://www.biogeosciences.net/6/849/2009/. 20808, 20809, 20817
Sofiev, M., Vankevich, R., Lotjonen, M., Prank, M., Petukhov, V., Ermakova, T., Koskinen, J., and Kukkonen, J.: An operational system for the assimilation of the satellite information on wild-land fires for the needs of air quality modelling and forecasting, Atmos. Chem. Phys., 9, 6833–6847, doi:10.5194/acp-9-6833-2009, 2009. 20808, 20809

ACPD
14, 20805–20844, 2014

Stehman, S. V., Olofsson, P., Woodcock, C. E., Herold, M., and Friedl, M. A.: A global land cover validation data set, II: Augmenting a stratified sampling design to estimate accuracy by region and land-cover class, Int. J. Remote Sens., 33, 6975–6993, 2012. 20817

van der Werf, G. R., Randerson, J. T., Giglio, L., Collatz, G. J., Kasibhatla, P. S., and Arellano Jr., A. F.: Interannual variability in global biomass burning emissions from 1997 to 2004, Atmos. Chem. Phys., 6, 3423–3441, doi:10.5194/acp-6-3423-2006, 2006. 20808

van der Werf, G. R., Randerson, J. T., Giglio, L., Collatz, G. J., Mu, M., Kasibhatla, P. S., Morton, D. C., DeFries, R. S., Jin, Y., and van Leeuwen, T. T.: Global fire emissions and the contribution of deforestation, savanna, forest, agricultural, and peat fires (1997–2009), Atmos. Chem. Phys., 10, 11707–11735, doi:10.5194/acp-10-11707-2010, 2010. 20808

Wiedinmyer, C., Akagi, S. K., Yokelson, R. J., Emmons, L. K., Al-Saadi, J. A., Orlando, J. J., and Soja, A. J.: The Fire INventory from NCAR (FINN): a high resolution global model to estimate the emissions from open burning, Geosci. Model Dev., 4, 625–641, doi:10.5194/gmd-4-625-2011, 2011. 20809

Wooster, M. J., Roberts, G., Perry, G. L. W., and Kaufman, Y. J.: Retrieval of biomass combustion rates and totals from fire radiative power observations: FRP derivation and calibration relationships between biomass consumption and fire radiative energy release, J. Geophys. Res., 110, D24311, doi:10.1029/2005JD006318, 2005.

ACPD
14, 20805–20844, 2014

Table 1. Bias and RMSE of mean global FRP in $mW\,m^{-2}$ for the year 2012 for Aqua and Terra GFAS with linear regression applied, as compared to Full GFAS, fixed and adaptive regions.

Satellite data assimilated	RMSE	Bias	Average FRP
Aqua and GFAS	0	0	0.0002238
Aqua (not corrected)	1.059×10^{-4}	-8.7611×10^{-5}	0.0003112
Terra (not corrected)	8.769×10^{-5}	7.541×10^{-5}	0.0001486
Aqua (fixed regions)	4.349×10^{-5}	-2.952×10^{-5}	0.0002536
Terra (fixed regions)	5.138×10^{-5}	3.304×10^{-5}	0.0001910
Aqua (adaptive regions)	2.599×10^{-5}	-1.876×10^{-6}	0.0002260
Terra (adapative regions)	4.515×10^{-5}	2.503×10^{-5}	0.0001991

ACPD
14, 20805–20844, 2014

Table 2. RMSE and bias of the regression applied to Aqua-GFAS as a function of the percentile of gridded FRP above which linear regression is applied instead of non-linear regression.

Percentile	RMSE	Bias	Average FRP
5	0.0001411	-3.683×10^{-5}	0.0002609
10	7.098×10^{-5}	-1.574×10^{-5}	0.0002398
15	6.312×10^{-5}	-1.017×10^{-5}	0.0002343
20	2.969×10^{-5}	-5.898×10^{-6}	0.0002300
25	2.8385×10^{-5}	-4.105×10^{-6}	0.0002282
30	2.693×10^{-5}	-2.722×10^{-6}	0.0002268
35	2.635×10^{-5}	-2.076×10^{-6}	0.0002262
40	2.609×10^{-5}	-1.639×10^{-6}	0.0002257
45	2.610×10^{-5}	-1.425×10^{-6}	0.0002255
50	2.608×10^{-5}	-1.259×10^{-6}	0.0002254
60	2.605×10^{-5}	-1.180×10^{-6}	0.0002253
100	2.599×10^{-5}	-1.876×10^{-6}	0.0002260

ACPD
14, 20805–20844, 2014

Table 3. RMSE and bias of the regression applied to Terra-GFAS as a function of the percentile of gridded FRP above which linear regression is applied instead of non-linear regression.

Percentile	RMSE	Bias	Average FRP
5	0.001114	−0.0002981	0.0005223
10	0.0003410	-8.815×10^{-5}	0.0003122
15	0.0002075	-3.897×10^{-5}	0.0002631
20	4.766×10^{-5}	-1.746×10^{-5}	0.0002416
25	4.183×10^{-5}	-1.239×10^{-5}	0.0002365
30	4.038×10^{-5}	-8.642×10^{-6}	0.0002327
35	3.916×10^{-5}	-4.957×10^{-6}	0.0002290
40	3.820×10^{-5}	-1.127×10^{-6}	0.0002252
45	3.758×10^{-5}	2.325×10^{-6}	0.0002218
50	3.725×10^{-5}	5.773×10^{-6}	0.0002183
60	3.828×10^{-5}	1.122×10^{-5}	0.0002129
100	4.515×10^{-5}	2.503×10^{-5}	0.0001991

ACPD
14, 20805–20844, 2014

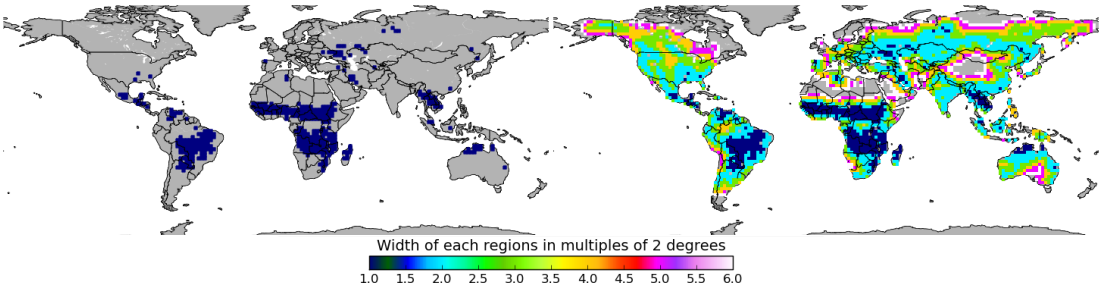

Figure 1. Width in multiples of 2° of every region with more than 400 positive 0.5° FRP grid cells from Terra and Aqua, in the period from 1 January 2003 to 31 December 2011. Fixed regions on the left, adaptive regionalization algorithm on the right.

ACPD
14, 20805–20844, 2014

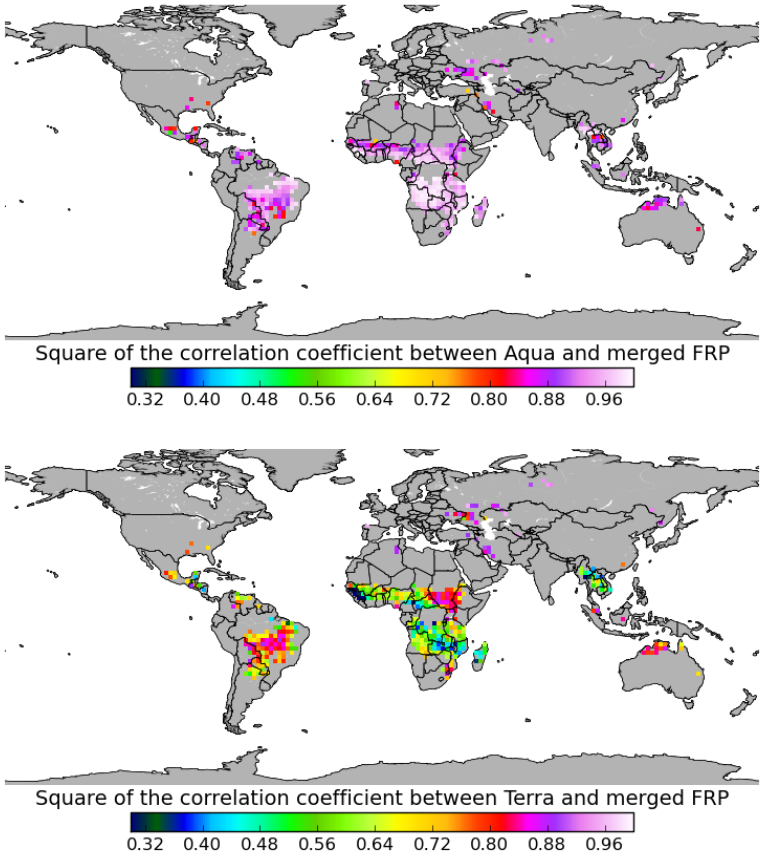

Figure 2. Square of the correlation coefficient between Aqua daily FRP (top), Terra daily FRP (bottom) and merged FRP. Fixed 2° × 2° regions were used.

ACPD
14, 20805–20844, 2014

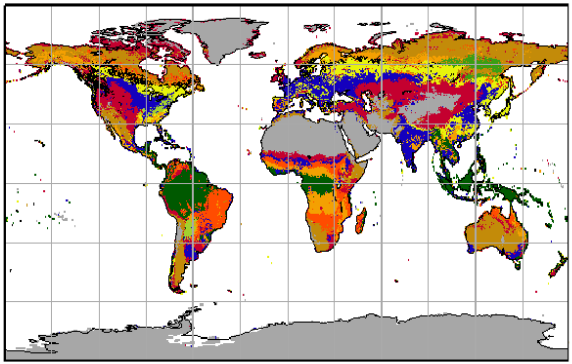

LCCAT	LC	Description	All
ENF	1	Evergreen needleleaf forest	2.8
EBF	2	Evergreen broadleaf forest	13.5
DNF	3	Deciduous needleleaf forest	1.5
DBF	4	Deciduous broadleaf forest	1.9
MF	5	Mixed forest	8.2
CSH	6	Closed shrublands	0.3
OSH	7	Open shrublands	20.7
WSA	8	Woody savannas	12.7
SAV	9	Savannas	11.4
GRA	10	Grasslands	20.2
CRO	12	Croplands	16.5
URB	13	Urban and built-up	0.6
BSV	16	Barren or sparsely vegetated	34.2
Sum		mio. km^2	144.8

Figure 3. Left, map of MCD12 (v5.1) land cover of the year 2005 (UMD classification) remapped to 0.1° using largest area fraction approach. Right, area in millions of km^2 of the UMD land cover classes.

ACPD
14, 20805–20844, 2014

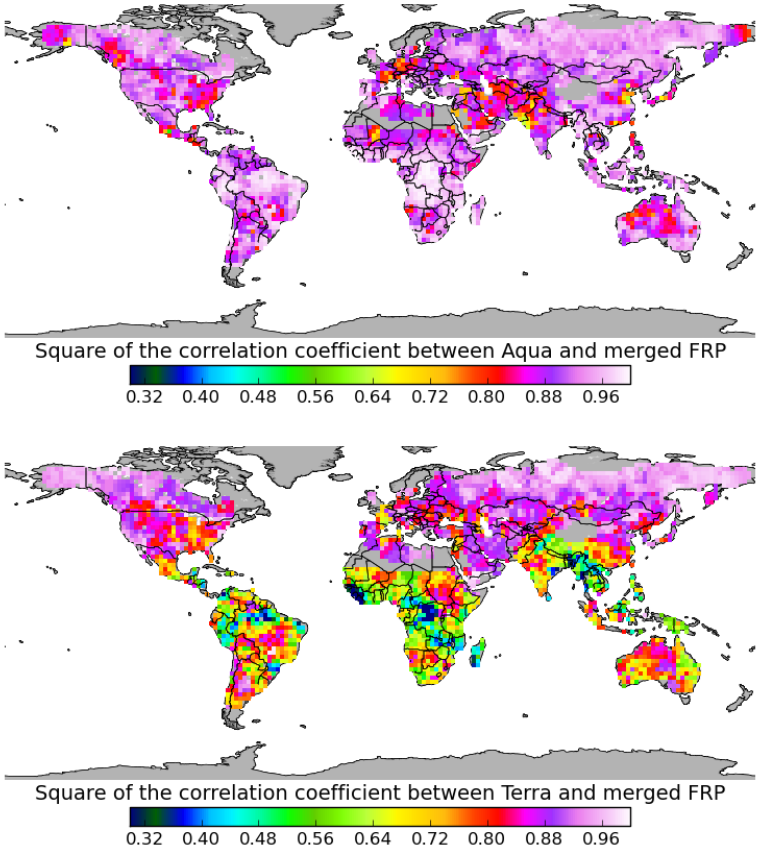

Figure 4. Square of the correlation coefficient between Aqua daily FRP (top), Terra daily FRP (bottom) and merged FRP with the adaptive regionalization algorithm.

ACPD
14, 20805–20844, 2014

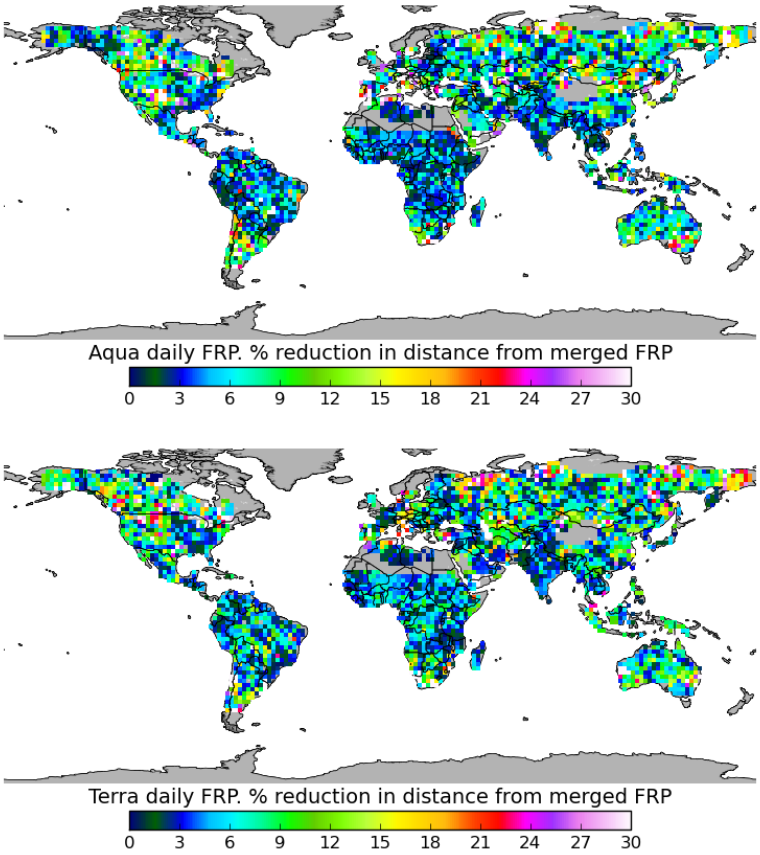

Figure 5. Reduction in percent of the distance between daily FRP from Aqua (top), Terra (bottom) and merged FRP by the nonlinear regression as compared to the linear regression.

ACPD
14, 20805–20844, 2014

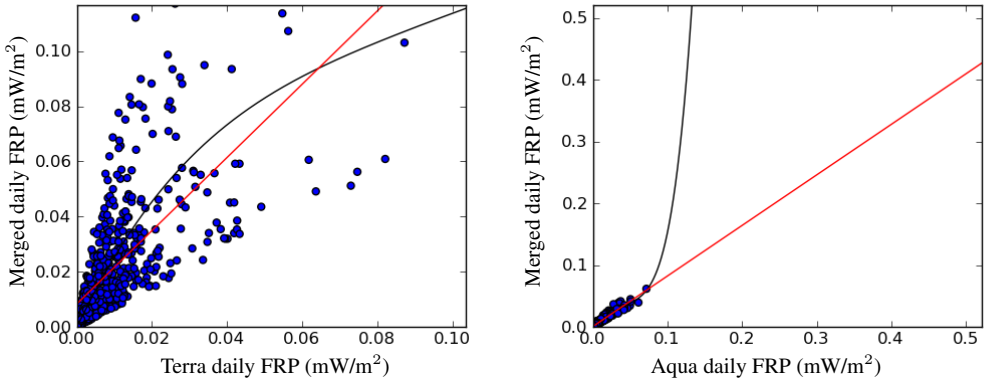

Figure 6. Scatterplot of Terra (left) and Aqua (right) daily FRP together with merged FRP. Linear regression between the two datasets is shown by a red line while the best fit non linear regression is shown in black. Regions considered are the square that extends from 24 to 26° E and from 16 to 18° S (left) and from 36 to 38° E and 58 to 60° N (right).

ACPD
14, 20805–20844, 2014

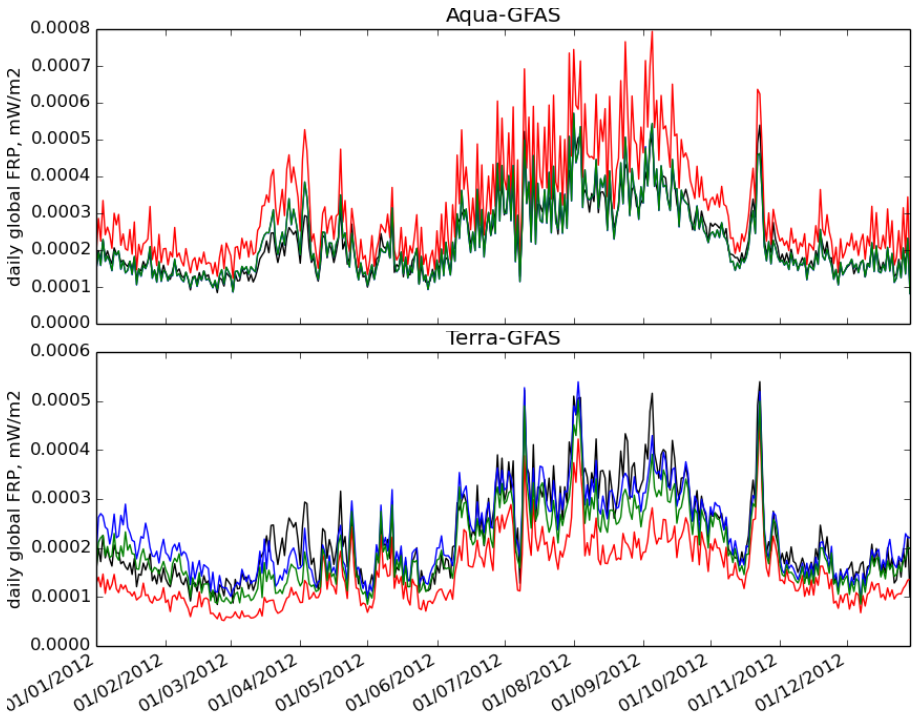

Figure 7. Daily global FRP from Aqua- and Terra-GFAS in red (Aqua on top, Terra, bottom), from Full-GFAS in black. Linear regression applied to Aqua- and Terra-GFAS is shown in green while the mix of linear on non-linear approaches is displayed in blue. Data from 1 January 2012 to 31 December 2012.

ACPD
14, 20805–20844, 2014

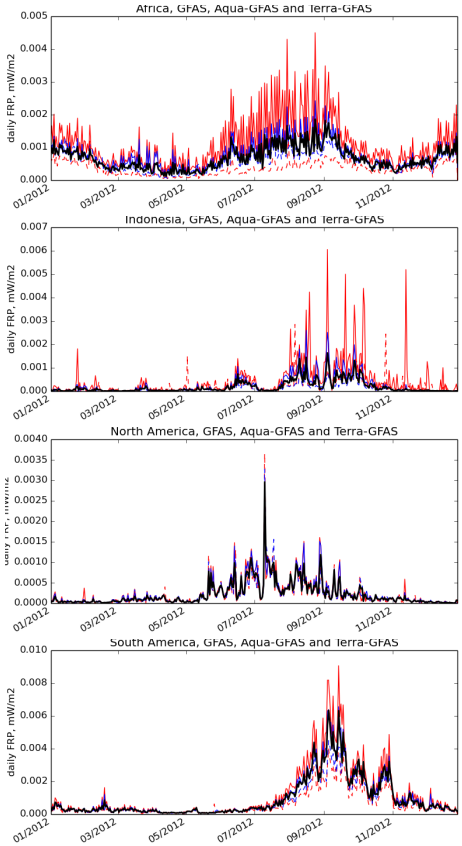

Figure 8. Daily FRP averaged of Africa (top), Indonesia (top middle), North America (bottom middle) and South America (bottom), for 2012. GFAS is in black, Aqua-GFAS (solid line) and Terra-GFAS (dashed line), using non corrected observations (red) and corrected observations (blue).

ACPD
14, 20805–20844, 2014

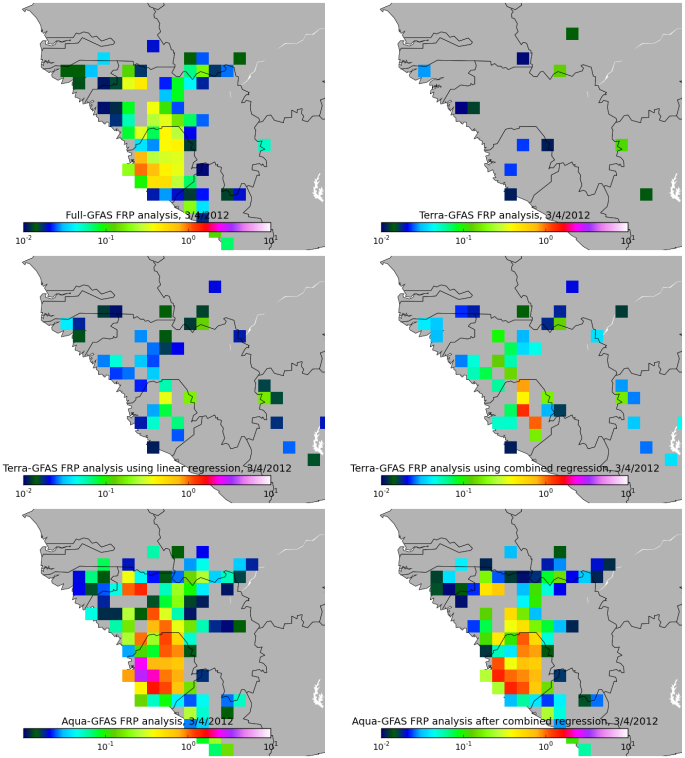

Figure 9. Daily FRP in $mW\,m^{-2}$ for West Africa on 3 April 2012, given by Full-GFAS (top left), Terra-GFAS (top right), Terra-GFAS using linear regression (middle left) and non-linear regression (middle right), Aqua-GFAS (bottom left) and Aqua-GFAS using non-linear regression (bottom right).

ACPD
14, 20805–20844, 2014

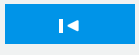

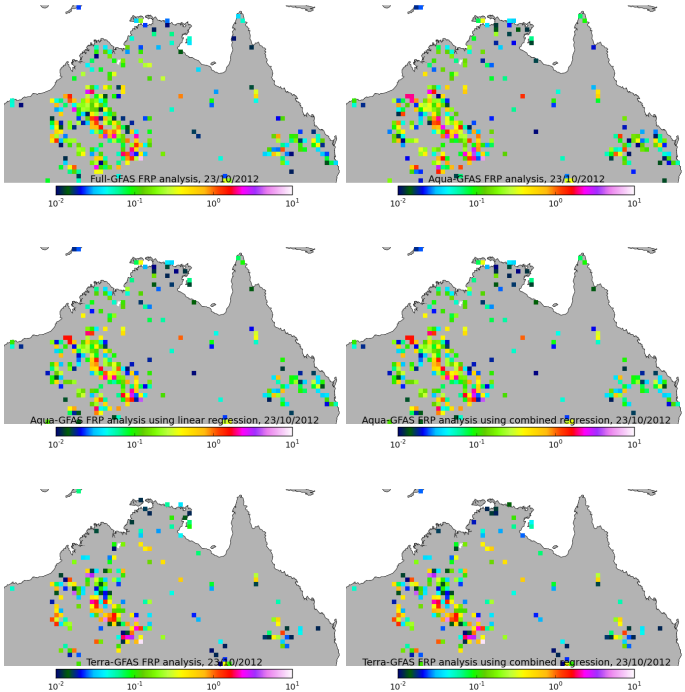

Figure 10. Daily FRP in $mW\,m^{-2}$ for Australia on 23 October 2012, given by Full-GFAS (top left), Aqua-GFAS (top right), Aqua-GFAS using linear regression (middle left) and non-linear regression (middle right), Terra-GFAS (bottom left) and Terra-GFAS using non-linear regression (bottom right).

ACPD
14, 20805–20844, 2014

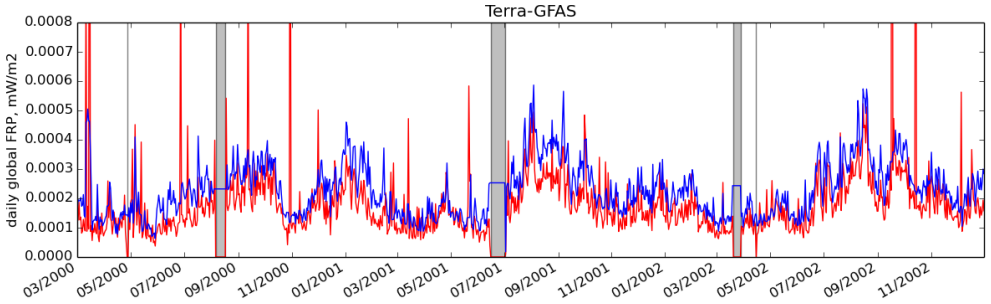

Figure 11. Daily global FRP from Terra-GFAS from 24 February 2000 to 31 December 2002, using non-corrected observations in red, using corrected observations in blue. The gray areas indicate that the MODIS/Terra observations were not available and that persistence was used instead in Terra-GFAS.

ACPD
14, 20805–20844, 2014

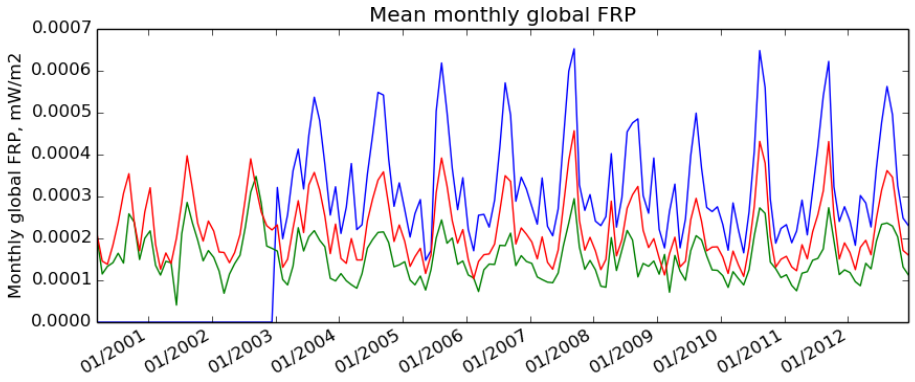

Figure 12. Monthly global FRP from Terra in green, from Aqua in blue, and from GFAS in red. Before 1 January 2003, GFAS is using Terra observations corrected with a combination of linear and non-linear regression, after 1 January 2003, GFAS is using observations from Aqua and Terra.

ACPD
14, 20805–20844, 2014